Composites Part C: Open Access 4 (2021) 100085

Contents lists available at ScienceDirect

Composites Part C: Open Access

journal homepage: www.elsevier.com/locate/jcomc

Steel foil reinforcement for high performance bearing strength in Thin-Ply composites☆

Benedikt Kötter[a,*], Kohei Yamada[b], Johann Körbelin[a], Kazumasa Kawabe[b], Masaaki Nishikawa[c], Masaki Hojo[c], Bodo Fiedler[a]

[a] Institute of Polymer and Composites, Hamburg University of Technology, Denickestraße 15, Hamburg 21073, Germany
[b] Industrial Technology Center of Fukui Prefecture, 61-10, Kawaiwashizuka, Fukui 910-0102, Japan
[c] Department of Mechanical Engineering and Science, Kyoto University, C3, Kyoto Daigaku-Katsura, Nishikyo-ku, Kyoto 615-8540, Japan

ARTICLE INFO

Keywords:
Fibre metal laminate (FML)
Hybrid material
Stress distribution
Open hole test
Digital Image Correlation

ABSTRACT

This study investigates the influence of local hybridization of Thin and Thick-Ply CFRP laminates on the open-hole and bearing properties. The area weight of the CFRP unidirectional prepregs used is 40 gsm in the case of Thin-Ply layers and 160 gsm in the case of Thick-Ply layers. The steel used is a 1.4310 stainless-steel foil with the same layer thickness as the prepregs. In the hybrid area, 90° layers were locally replaced by stainless steel patches. The local metal foil content varies from 6.25%, 12.5% to 25.0%. For notched laminates, the open hole tensile strength is significantly decreased with thinner layer thicknesses. The failure behavior changes from complex delamination dominated failure to brittle failure. By using stainless steel foils in the regions of stress concentrations, energy can be dissipated by plastic deformation of the steel foil and stresses can be deflected to neighbouring areas. For Thin-Ply samples with a local steel content of 25% the open hole tensile strength increases by 64% in comparison to the reference Thin-Ply specimens and the sensitivity towards stress concentrations decreases. The bearing strength of the hybrid CFRP laminates is increased by up to 54.6% in comparison to the reference material, due to the confinement of the steel foil and the resulting higher compressive strength and the plastic deformation at high stresses. The stress–strain diagrams and micrographs of the fibre metal samples reveal that damage is initiated before the maximum bearing strength. However, the damage offset bearing strength increase concerning the specific density of the material significantly.

1. Introduction

Due to the excellent density-specific mechanical properties, carbon fibre reinforced composites (CFRPs) are often used as a structural material for lightweight structures [1]. However, conventional CFRP laminates or structures do not exploit the full potential of the used carbon fibres. One approach to improve their performance is to reduce the layer thickness. Kawabe et al. and Sihn et al. presented a spread-tow process to produce thin unidirectional plies, so-called Thin-Ply layers as low as 20 μm [2,3]. As a result, the degree of freedom in design increases with decreasing layer thickness due to the larger number of used plies or more precise load-dependent design.

The failure behavior is highly dependent on the layer thickness, a decreased layer thickness suppresses transverse microcracking and free edge delamination due to an increase of transverse tensile strength (in-situ effect) [4]. The failure mode changes from complex delamination dominated failure to a brittle failure from Thick- to Thin-Ply [3–7], which results in a higher ultimate tensile strength for unnotched quasi-isotropic specimens [3,6,8]. In addition to the improvement of the mechanical properties due to the in-situ effect, the laminate quality improves with regard to void content, fibre angle deviation and resin rich areas with decreasing layer thickness. This can be attributed to the spreading process, which results in a more homogeneous fibre distribution. Due to these factors, the compressive strength of unidirectional Thin-Ply samples increases compared to thicker layers [6,8].

In contrast to the unnotched samples, notched Thin-Ply specimens exhibit a lower open hole tensile strength. As a consequence of the suppression of inter-fibre fracture and delamination, no crack blunting of the stress concentration due to interlaminar damage occurs. Thus, no energy can be dissipated or stress diverted to adjacent areas and no predamage leads to premature fibre failure at the notch or stress concentration region [3,6,7]. In order to reduce the notch sensitivity, the material

☆ This work was financial supported by the “Der Übersee-Club e.V.”, Hamburg, Germany. Thanks to Aviatec Gobal Aviation GmbH & Co. KG, Henstedt-Ulzburg, Germany for supplying surface pre-treatment systems

* Corresponding author.
E-mail address: benedikt.koetter@tuhh.de (B. Kötter).
URL: http://www.tuhh.de/kvweb (B. Kötter)

https://doi.org/10.1016/j.jcomc.2020.100085
Received 13 October 2020; Received in revised form 7 December 2020; Accepted 8 December 2020

Table 1
Laminate layups and global specimen densities for the open hole tensile (OHT) and bearing tests.

Configuration (SF: Steel Foil)	Density in g/cm³		Layup
	OHT	Bearing	
CFRP: 40 gsm; Reference	1.53	1.53	$[45/90/-45/0]_{12s}$
CFRP: 40 gsm; SF 6.25 %; (t = 0.04 mm)	1.62	1.67	$[(45/SF/-45/0)_3/(45/90/-45/0)_9]_s$
CFRP: 40 gsm; SF 12.5 %; (t = 0.04 mm)	1.70	1.80	$[(45/SF/-45/0)_6/(45/90/-45/0)_6]_s$
CFRP: 40 gsm; SF 25.0 %; (t = 0.04 mm)	1.86	2.07	$[45/SF/-45/0]_{12s}$
CFRP: 160 gsm; Reference	1.53	1.53	$[45_4/90_4/-45_4/0_4]_{3s}$
CFRP: 160 gsm; SF 25.0 %; (t = 0.16 mm)	1.88	2.12	$[45_4/SF/-45_4/0_4]_{3s}$

can be modified in such a way that the entire failure mechanism changes and, for example, micro-damages occur. One possibility is to introduce a second material (hybridization), allowing synergy effects to be used in customized designs depending on the load situation such as notches or load introduction areas. In this study, the approach is to locally substitute 90° CFRP layers with stainless steel foils in the area of stress concentration. Stainless steel is less sensitive to stress concentrations due to their isotropic material and strain hardening properties.In contrast to titanium or aerospace aluminium alloys, stainless steels are more economical [9]. Due to hybridization with stainless steel, the failure behavior changes from a brittle failure back to a complex multi-mode failure. Previous studies which have investigated carbon fibre reinforced Thin-Ply laminates with stainless steel patches show higher open hole tensile strengths [10,11], which increased from 390 MPa to 630 MPa with a local steel content of 25%, an increase of about 60.44%. Although the global density of the specimen increases due to hybridization, the density specific strength is nonetheless increasing and the notch sensitivity is reduced. Local thickening or other design features can be minimized or eliminated. Previous studies encountered stress concentrations in the transition zone caused by the difference in stiffness of CFRP and stainless steel. Therefore the stainless steel patches were arranged step-wise. As a result, the increased stresses are distributed over a wider area, and locally the stress concentration decreases [11]. The staircase arrangement has also been used in other works [12–14].

Another field of application for hybrid CFRP laminates is fastener-based joints. Bolt or rivet joints are the most commonly used type of joining techniques today due to their simple application, low price and the possibility of release [15–17]. However, this type of joint is not appropriate for the use of CFRP. A study by Amacher et al. showed that the bearing strength of Thick-Ply samples is 20% lower than the unnotched tensile strength. In the case of thin-layer specimens, the reduction was 31%, whereby the absolute bearing strength of 584 MPa for Thin-Ply is higher than the bearing strength of 476 MPa for Thick-Ply samples [4,6]. The bearing strength of Thin-Ply is higher, however the difference between unnotched and bearing strength is greater, which is limiting the potential of Thin-Ply. As a result the joints have to be improved. The use of stainless steel layers could reduce the gap between tensile strength and bearing strength and thus prevent solutions such as local thickening of the laminate [18], placing inserts such as metallic rings [16] or Z-pinning [19,20]. The frequently used local thickening has the disadvantage that bending stresses and peel stresses are introduced into the material, which can be prevented by hybridisation while retaining the original geometry. Petersen et al. investigated the transition zone (TZ) between stainless steel and CFRP layers for unnotched tensile and bending samples [21]. The layers used had a thickness of 0.13 mm. Four different arrangements of the metal in the transition zone were investigated. It was observed that delamination between matrix and stainless steel is a challenge in the TZ [21]. With reduced layer thickness, the number of layers increase, which decreases the interlaminar shear stresses caused by thermal and mechanical loads, which reduces and suppressed the growth of delaminations. As a consequence, the requirements of the bonding between resin and metal are, therefore, less critical. Well-known solutions such as the Boeing Sol-Gel process are sufficient and no further investigations are necessary [11,22]. Other work has focused on the influence of the fastening torque on the bearing strength and the failure behavior of the specimen. Whether the bolt is tightened or not and with which torque it is tightened has a significant influence on the bearing strength. In general, higher tightening torques increase the bearing strength, as long as the tightening does not damage the specimen [12,23–25].

2. Materials and methods

2.1. Materials and specimen preparation

The prepreg system used in this study was manufactured by the spread tow technology at the Industrial Technology Center of Fukui Prefecture, Japan. TR50S carbon fibres from Mitsubishi Chemical Co., Ltd. and a bisphenol-A based epoxy resin from a combination of jER828:jER1001 in a 4:6 ratio from Mistubishi Chemical Co., Ltd. was used. The area weight of the prepreg layers was 40 gsm. Thick-Ply laminates with a resulting area weight of 160 gsm were produced using the block-scaling method. The fibre volume content of the produced laminates is 55%. As substitute layers, the austenitic stainless steel alloy 1.4310 (X10CrNi18-8) from h+s Präzisionsfolien GmbH, Pirk bei Weiden, Germany were used. The alloy 1.4310 is characterized by high strength and ductility, and exhibits good corrosion properties. The thicknesses of the foils are the same as the prepreg layers. The strength of the Thin-Ply metal foil is higher than the strength of the Thick-Ply foil due strain hardening from the cold rolling during manufacturing. The foils are cut using a precision cutter for electrical boards. This cutting method prevents warping edges and therefore additional weak points in the materials. Table 1 displays the local volume content of stainless steel near the hole and the global specimen density. In contrast to the local steel content, the global density is calculated over the entire sample, as the patches are only applied locally, even in practical use. If the steel content is lower than 25%, the outer 90° layers are replaced by steel foils symmetrical to the mid-plane, because due to the clearance fit between bolt and hole the bolt inclines under load and the outer layers are loaded under pressure. In order to minimize a local stiffness increase by inserting stainless steel instead of 90° CFRP layers, the steel patches have a different length, and their design is stepwise, as shown in Fig. 1.

The laminates are manufactured by a hand layup and an intermediate vacuum was applied every fourth layer. A high-performance sol-gel surface pre-treatment process using 3M's (Germany) AC-130-2 surface pre-treatment system, an aerospace certified two-part water-based system without chromate, was applied to increase the adhesion between stainless steel and matrix. The pre-treatment system improves the adhesion as a result of the chemical interaction at the interface between stainless steel and the matrix [22]. The process consists of four steps [22]:

1. Deoxidizing and extending the surface manually of the metal with # 500 abrasive paper.
2. Cleaning of the surface with acetone to remove all metal and abrasive parts and mixing the AC-130-2 Sol-Gel Kit.
3. Applying the surface pre-treatment by immersion bath for 2 min.
4. Drying of the coated surface for at least 60 min.

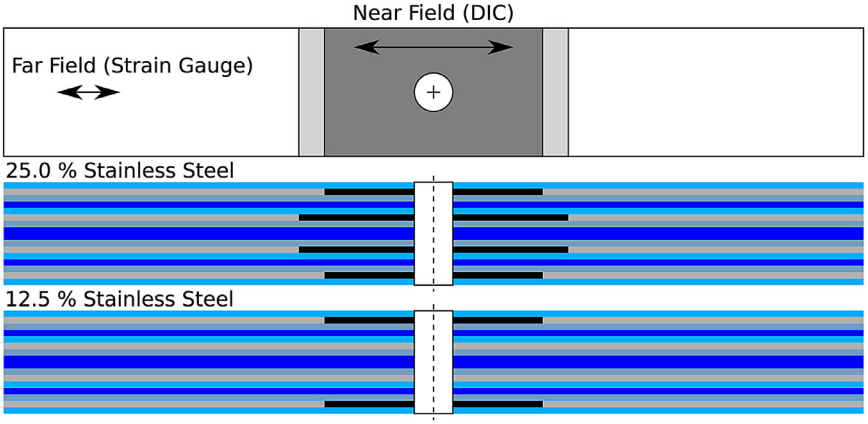

Fig. 1. Open hole tensile specimen geometry with a local steel content of 25% and 12.5%.

Table 2
Open hole tensile and bearing specimen dimensions [26,27].

Specimen dimension	OHT specimen in mm	Bearing specimen in mm
Hole diameter, *d*	6 ± 0.06	6 +0.00/−0.03
Thickness, *t*	3.84	3.84
Length, *l*	250	135
Width, *w*	36 ± 1	36 ± 1
Edge distance, *e*	125 ± 0.12	18 ± 1

The patches are inserted manually during lamination and the laminates are cured in an autoclave at 130 °C and 5 bar for 2 h. The cured plates were cut with the circular saw Brillant 265 from ATM with a Corundum blade and a constant feed speed of 1.5 mm/s. The hole was milled using a double-edged diamond milling cutter with a diameter of 1.8 mm. The specimen dimensions are determined according to the standards for OHT (ASTM D5766 [26]) and for Bearing (ASTM D5961 [27]) tests. All specimen dimensions are showed in Table 2.

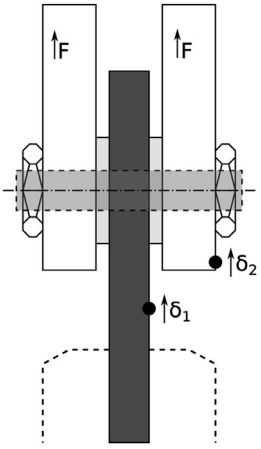

Fig. 2. Test setup double-shear bearing test.

2.2. Experimental methods

The open hole tension tests according to ASTM D5766 [26] were carried out in two different labs. Of the 24 samples tested, 6 were tested in Japan at Shimadzu's test laboratory in Kyoto, Japan. A shimadzu AG-X plus universal test machine with a maximum tensile force of 250 kN and mechanical wedge clamps was used. Far-field strain recording was performed using strain gages, near-field recording using a Digital Image Correlation (DIC) system (5M system) from GOM GmbH, Germany. The near-field displacements and strains were recorded using a speckle pattern, which was applied to the surface of the specimen using white and black acrylic paint. The evaluation of the data was carried out by the software ARAMIS Professional, which is distributed by GOM GmbH. The remaining open hole tension tests and the bearing tests according to ASTM D5961 [27] are conducted in Hamburg, Germany. For the investigations in Hamburg a ZwickRoell Z400 universal testing machine with a maximum load of 400 kN was used. The specimens were clamped using mechanical wedge clamps. The test parameters were adapted to the corresponding standard so that the results are comparable with the data from Japan or other studies. The tests in Japan as well as in Hamburg were performed under standard climate conditions of 20 °C and 50% humidity.

The procedure A "Double Shear Test" according to ASTM D5961 [27] was chosen for the bearing tests. The fastening torque was set to 3 Nm. Previous investigations have demonstrated that if the high-strength bolts are not tightened, they will fail before the hybrid FML specimen. Therefore no prediction of the bearing strength will be possible. The clamping pressure was applied to the sample using a steel washer with an inner diameter of 6.3 mm and an outer diameter of 12 mm. In the case of bearing tests, the calculation of the strains results from the local displacements of the sample and the upper clamping system. The calculation of the bearing strain ε^{br} is shown in Formula 1. δ_1 and δ_2 are the local displacements as it is shown in the schematic test setup in Fig. 2, K is the calculation factor to distinguish single-shear from double-shear tests. For single-shear tests the K is 1.0. D is the diameter of the hole.

$$\varepsilon^{br} = \frac{(\delta_1 + \delta_2)/2}{K \cdot D} \tag{1}$$

The bearing strength σ^{br} is calculated according to Formula 2. P is the load, h is the specimen thickness and k is the load per hole factor; 1.0 for single-fastener or pin tests and 2.0 for double-fastener tests.

$$\sigma^{br} = \frac{P}{k \cdot D \cdot h} \tag{2}$$

To be able to assess the failure mechanisms, micrographs of the tested samples were prepared. Samples up to the final failure, as well as samples up to a stress of 95% of the maximum stress, were examined. For this purpose, the samples were first embedded in coloured epoxy resin to prevent further damage during sawing of the samples. After sawing, the specimens were embedded in a cold embedding material (KEM 15 plus from ATM Qness GmbH) and automatically ground and polished. The polishing process consists of several steps, starting with #320 abrasive paper to a diamond suspension with a grain size of 1 µm. The polished surfaces were observed with the digital microscope from KEYENCE.

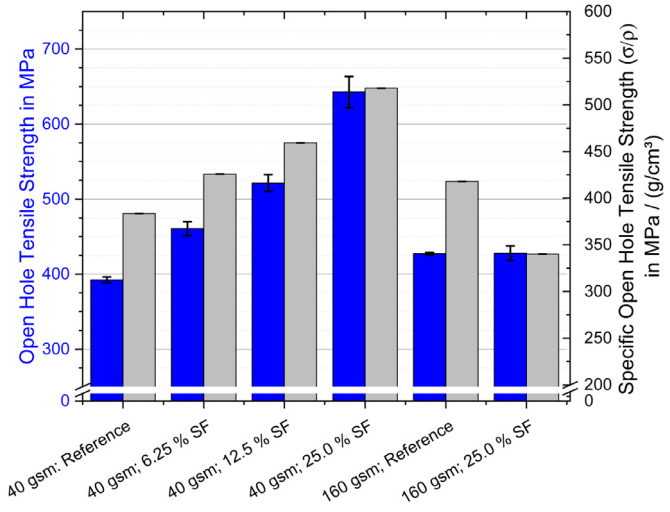

Fig. 3. Open hole tensile strength (blue) and density specific open hole tensile strength (grey) of CFRP and Hybrid CFRP fibre metal laminates.

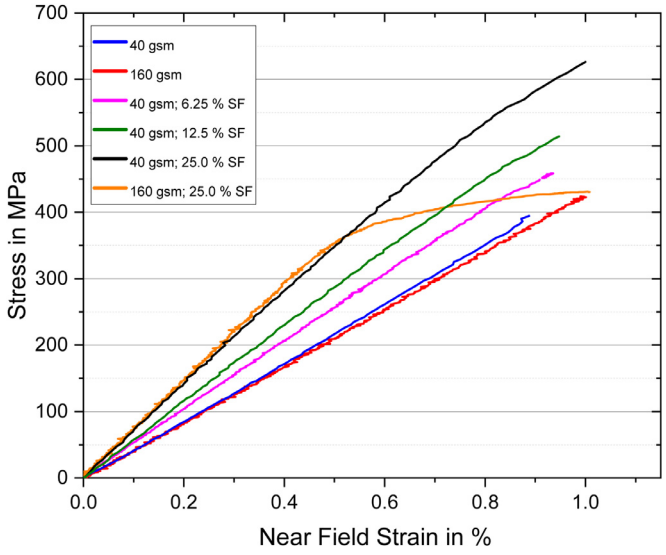

Fig. 4. Stress–strain-diagram of the open hole tensile tests.

3. Results and discussion

3.1. Open hole tensile tests

Fig. 3 shows the results of the open hole tensile tests. The strength is illustrated in blue, and the specific strength in grey. The specific strength represents the ratio of the strength and the global density of the sample. Therefore, Thick-Ply samples with a local steel content of 25% have a density of 1.88 g/cm^3 in contrast to the reference samples with a density of 1.53 g/cm^3. The corresponding densities of the samples are summarized in Table 1. The open hole tensile strength of the Thin-Ply samples recorded a 9% lower strength than the Thick-Ply specimens. This corresponds to other studies which had investigated the OHT strength concerning the layer thickness [3,6,11]. Amacher et al. showed that initial damage in the material shifts to higher strains or stresses with decreasing layer thickness. The onset of damage increased from 255 MPa for Thick-Ply specimens to 352 MPa for Thin-Ply specimens. Due to the delayed onset of damage, the lack of stress relaxation through damage leads to higher stress concentrations and premature, brittle failure [3,6,7].

The ultimate strength increases significantly with increasing steel content. With a local steel content of 25%, the strength rises by 64%, and even the specific strength rises by up to 36%. Due to the hybridization, the notch sensitivity decreases with an increase in steel content. The reduction in notch sensitivity is expressed in a decreasing notched strength reduction ratio (NSR). The NSR indicates the ratio between the notched strengths σ_{UNT} and the middle stress in the net section σ_{net}. The stress in the net section is calculated from the OHT strength σ_{OHT}, the specimen width W and the hole diameter D, see Eq. (3) [7].

$$NSR = \frac{\sigma_{UNT}}{\sigma_{net}} = \frac{\sigma_{UNT}}{\sigma_{OHT}/(1-\frac{D}{W})} \quad (3)$$

A value of nearly one indicates that the stress concentration has only a minimal influence on the strength, whereas higher values indicate high sensitivity to stress concentrations. The measured values are shown in Table 3. It can be seen that the NSR decreases with increasing steel content, thus reducing the susceptibility to stress concentrations. In the case of the Thin-Ply FML samples with a steel content of 25%, the NSR value is 1.18. As a result, areas with high-stress concentrations have only a small influence, and no thickening or other design changes need to be made locally. The local hybridisation of the material avoids the problem of the influence of stress concentrations in thin-layer laminates so that the potential of the thin layers can be exploited. The right bar of Fig. 3 displays the results of the Thick-Ply samples with a local steel content of 25%. A decrease in strength is shown in contrast to the Thin-Ply samples with 25% steel content. The lower strength can be explained by the formation of delaminations between the metal layers and the matrix. Due to the higher shear stresses between the layers compared to Thin-Ply, the chosen surface pre-treatment is not sufficient, and delaminations are formed. Higher shear stresses result partly from the mechanical loads introduced and partly from the residual stresses in the laminate. In the case of the interface between stainless steel and CFRP, and the large difference in the coefficient of thermal expansion, the residual stresses between them are higher. This consideration favours the formation of delamination. The formation of delaminations can be seen in the stress-strain diagram (Fig. 4) by a decrease in stiffness at about 340 MPa.

On the abscissa, the near-field strain is plotted, which was obtained using the Digital Image Correlation system. Near field Strain was recorded over a length of 35 mm, so that only the area with the maximum stainless steel content depending on the sample is measured. The measuring field is on the left side of the hole and was chosen to ensure that local effects of the hole have no influence (Fig. 1). Except for the Thick-Ply specimen with a local steel content of 25%, all specimens exhibit brittle failure and no major significant pre-damage. The difference

Table 3
Notched strength reduction ratio of the Thin- and Thick-Ply FML samples.

Configuration (SF: Steel Foil)	Strength in MPa		NSR
	Unnotched	Open hole tension	
CFRP: 40 gsm; Reference	911.97 ± 34.43	392.41 ± 3.84	1.94
CFRP: 40 gsm; SF 6.25 %; (t = 0.04 mm)		460.78 ± 9.23	1.65
CFRP: 40 gsm; SF 12.5 %; (t = 0.04 mm)		521.41 ± 11.25	1.46
CFRP: 40 gsm; SF 25.0 %; (t = 0.04 mm)		642.78 ± 20.67	1.18
CFRP: 160 gsm; Reference	857.21 ± 11.06	427.27 ± 1.67	1.67
CFRP: 160 gsm; SF 25.0 %; (t = 0.16 mm)		428.02 ± 9.70	1.67

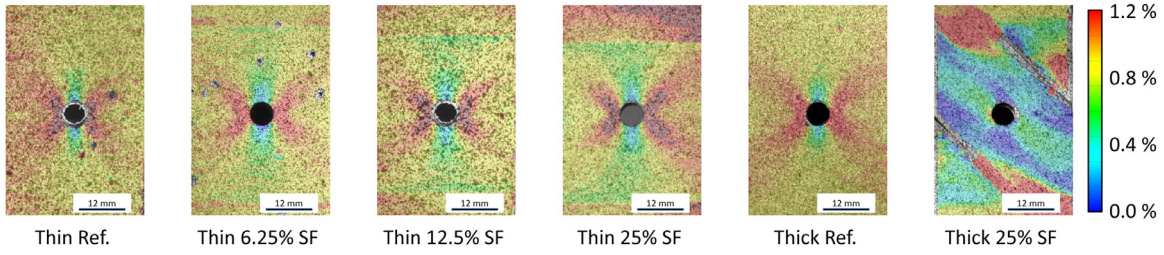

Fig. 5. Strain in tensile direction shortly before final failure recorded by a DIC system.

Table 4
Theoretical and measured stiffness of the hybrid area. The stiffnesses of the reference samples (italics) were determined by measurements according to ASTM D3039.

Configuration	Measured stiffness in GPa	Theoretical stiffness in GPa
40 gsm	43.57 ± 0.91	*47.00 ± 0.67*
40 gsm; 6.25% SF	51.38 ± 0.39	50.23
40 gsm; 12.5% SF	57.00 ± 1.04	56.89
40 gsm; 25.0% SF	69.43 ± 0.35	70.20
160 gsm	42.70 ± 0.37	*47.87 ± 1.49*
160 gsm; 25.0% SF	74.13 ± 4.06	70.20

in the stiffness can be explained by the local steel content. The steel layers replace 90° layers of CFRP, which have a lower tensile stiffness than the steel foil. The measured stiffnesses correspond to the theoretically calculated stiffnesses if the rule of mixture and the local steel content are used. The stiffnesses of the individual materials is based on tensile tests for quasi-isotropic CFRP samples according to the ASTM D3039 [28] and tensile tests for the steel foil according to the ASTM E345-16 [29]. The measured and calculated stiffnesses are shown in Table 4.

The Far-Field strain was recorded outside the area of local hybridization using strain gauges, and the stiffnesses were determined. As expected, no near field stiffness differences between the configurations can be detected, since the stiffness is influenced by the fibres and resin and not by the layer thickness. The stiffness is the equivalent to the near field stiffness of the notched reference samples.

The DIC images in Fig. 5 show the surface strains of the top 45° layer in tensile direction right before final failure. Except for the right specimen (Thick-Ply, 25% SF), all samples show a typical stress pattern near the hole for quasi-isotropic open hole tension specimens. A stress concentration propagates from the hole in ±45°, furthermore above and below the hole, a local stress minimum appears.

Furthermore, it is visible that with increasing steel content, the transition zone between CFRP and stainless steel is more clearly visible and the stress concentrations at the transition zone increase. Thus, the transition zone in addition to the hole represents a second critical area with respect to specimen failure. Fig. 6 illustrates two curves, representing the strain in tensile direction as a function of position. The position data is a vertical section through the sample, where 0 mm represents the centre of the sample, i.e. the centre of the hole (see Fig. 6 top right). The strains in the diagram belong to a farfield tensile stress of 350 MPa at which delamination growth begins in the hybrid Thick-Ply specimens. The strain curve (orange) of the Thick-Ply specimen with a local steel content of 25% shows two strong stress peaks symmetrical to the middle. These are located at the transition between the outer metal layers and the corresponding 90° CFRP layers. The local increase of stress initiates delamination growth and results in early failure. In the case of the hybrid Thin-Ply specimens with a steel content of 25% (black), no strong localized stress increase is observable. Due to the low layer thickness, more metal layers are required, which in turn can be distributed more smoothly in steps. This ensures that the stress increase is distributed over a larger area, and therefore the local stress concentrations decreased. The specimen fails at the hole, as do the reference specimens.

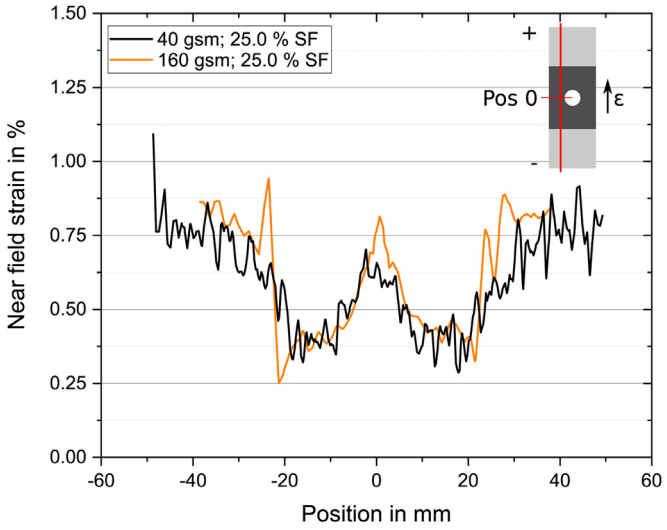

Fig. 6. Near field strain in tensile direction as a function of the position on the specimen.

In addition to the DIC images, micrographs of the fracture surfaces of the specimens were produced. The images a) to d) of Fig. 7 show micrographs of Thin-Ply specimens next to the hole. As the curves of the stress-strain diagram have already shown, brittle material behavior can also be seen here. Especially the Thin-Ply specimen without stainless steel foil (Fig. 7a) shows a very straight fracture surface. Areas with stainless steel foils show a rougher fracture surface. The length of the fracture surface increases significantly. Fig. 7e and f shows detailed images of the fracture edges. An explanation for the higher fracture surfaces in the hybrid areas is the higher fracture strain and plastic deformation of the stainless steel. Due to the higher strains, more inter-fibre fractures in the CFRP layers occur before ultimate failure. These fractures do not always occur at the same location but are statistically distributed. Right before ultimate failure, the individual layers are pulled out, similar to the pull-out of fibres. This ensures that additional energy is dissipated and the open hole tensile strength increases. A characteristic of localized high plastic strains in metal materials is the fracture angle of the metal. In Fig. 7 e it can be seen a ductile failure behavior of the metal foil. In order to be able to examine the inter-fibre fractures more precisely, samples were loaded up to a maximum stress of 95% of the ultimate strength, and further micrographs were prepared. These are shown in Fig. 7 g and h. However, no damage to the material has yet been detected. Nevertheless, it can be seen that no resin-rich regions or voids are introduced into material due to the introduction of metal layers. Furthermore, there are no delaminations in the laminate between the metal and the CFRP due to the thermal stresses. Delaminations are only on the most outer metal layers. However, since DIC detected no deformation perpendicular to the surface of the specimen, the outside delaminations are a result of the compressive stresses occurring within the specimen after the final fracture.

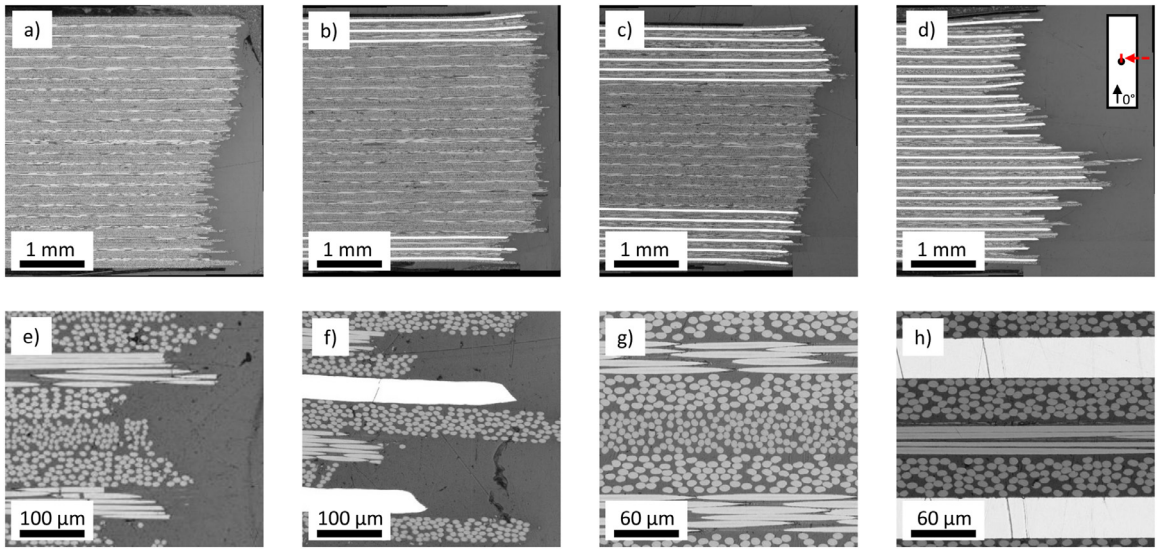

Fig. 7. A to F: Micrographs of the fracture surfaces of the open hole tensile specimens; G and H: Micrographs of two specimens loaded to 95% of the maximum strength.

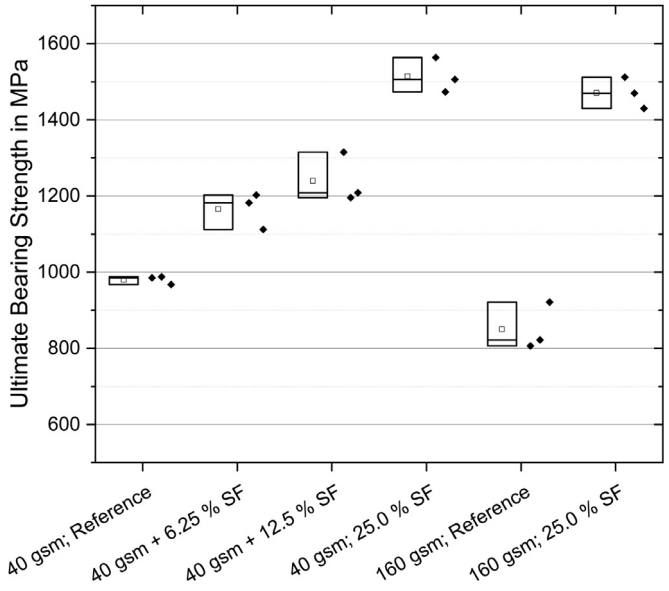

Fig. 8. Results of the maximum bearing strength regarding layer thickness and steel content.

3.2. Bearing strength

In the following section, the results from the bearing tests are presented. Fig. 8 demonstrates the bearing strengths of the six configurations. As with the open hole tension tests, three samples were tested per configuration since the results showed a significant difference. Higher bearing strengths are achieved with decreasing layer thickness. The bearing strength increases by 15.3% from 849.85 MPa (Thick-Ply) to 979.61 MPa (Thin-Ply) with a reduction of the area weight from 160 gsm to 40 gsm. Previous studies by Masania et al. and Amacher et al. show that the use of thin layers influences the bearing damage mechanism [6,10]. The onset of first damage shifts to higher stresses and strains and the initiation and propagation of delamination as well as matrix cracks are suppressed. Furthermore, the intra-laminar shear stresses are lower due to the thin layer thicknesses, which according to Garbo et al. [30], results in a delay in the initiation of damage mechanisms such as matrix breakage, fibre kinking and through-thickness shear cracking. Which, as a result, increases the bearing strength. However, the disadvantage is that progressive behavior is no longer present and the stress reduction after initial damage is very large. For safety-relevant components, such as in aircraft structures, this is particularly critical [6,31,32].

The micrographs in Fig. 9 show the damage pattern of tested and embedded samples. Fig. 9a and d shows overview images of the loading area of thin layer (a–c) and thick (d–f) specimens. In the case of Thin-Ply specimens, fewer delaminations occur, and the samples show less damage after loading. Noticeable for the thin layer thicknesses are the fibre breakage within the 0° layers (Fig. 9b) and (global kink bands (Fig. 9 c), which increase from the centre outwards. The clamping area of the washer is visible as a flat area beside the hole (blue lines in Fig. 9, directly behind this clamped areas global buckling occurs, which results in fibre breakage and final failure. Fibre breaks within the 0° layers indicate large compressive stresses. Due to the low layer thickness, the bending stiffness of the specimen is only slightly reduced, with fracture of a single 0° layer. Due to the remaining residual stiffness and the clamping by the washer, no global buckling occurs. Concerning regions far away from stress concentrations, no damage is spreading further. The area affected by damage resulting from the Bearing load damage is considerably smaller in the Thin-Ply specimen. In contrast, large delaminations between the layers can be seen in the Thick-Ply sample. Although the support of the first area (blue lines in Fig. 9a and d) does not cause any buckling either, the complete sample fails within this area. The individual layers have fractured in numerous fragments and have shifted due to the delamination. This behavior can also be seen in the two detailed images in Fig. 9 e and f. Due to the fractures and the displacements, no global Kink bands can be observed. Regarding the more distant areas, external delamination has continued, and the outer 45° layer has detached.

Due to the hybridization with stainless steel foils, significantly higher bearing strengths can be observed (see Fig. 8). In contrast to the Thin-Ply samples with a bearing strength of 979.6 MPa, the strength of the samples with stainless steel foil increases to 1165.4 MPa in the case of 6.25% stainless steel, via 1239.5 MPa in the case of 12.5%, to 1513.9 MPa MPa if all 90° layers are replaced by stainless steel (25%), which corresponds to an increase of 54.6%. In the case of the Thick-Ply fibre metal specimens, the bearing strength increases to 1470.6 MPa, an increase of 73%. In addition to the increased bearing strength, however, the occurring damage mechanism changes. The corresponding stress-strain diagrams are shown in Fig. 10. One representative sample is shown for each configuration. In addition to the fact described above that the Thick-

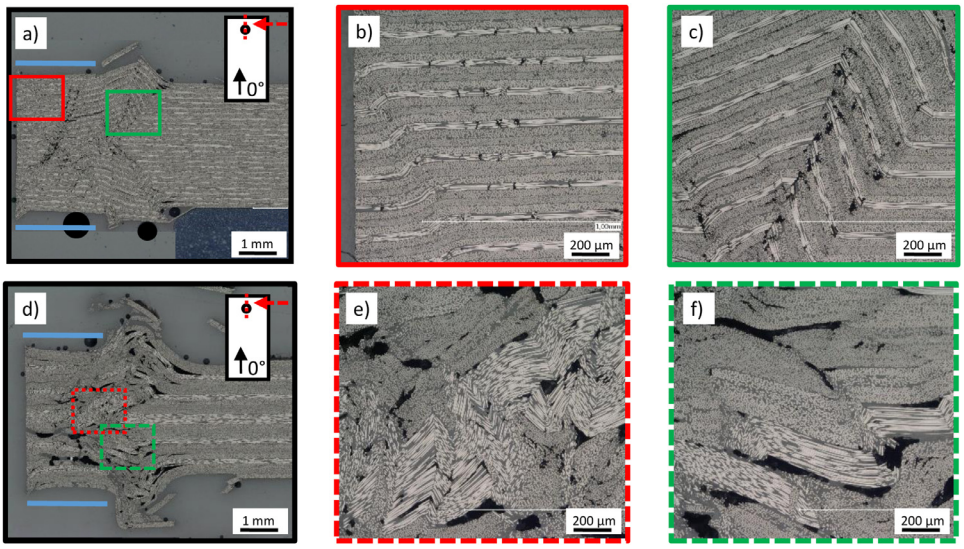

Fig. 9. Micrographs of bearing Thin- (upper micrographs) and Thick-Ply (lower micrographs) specimen.

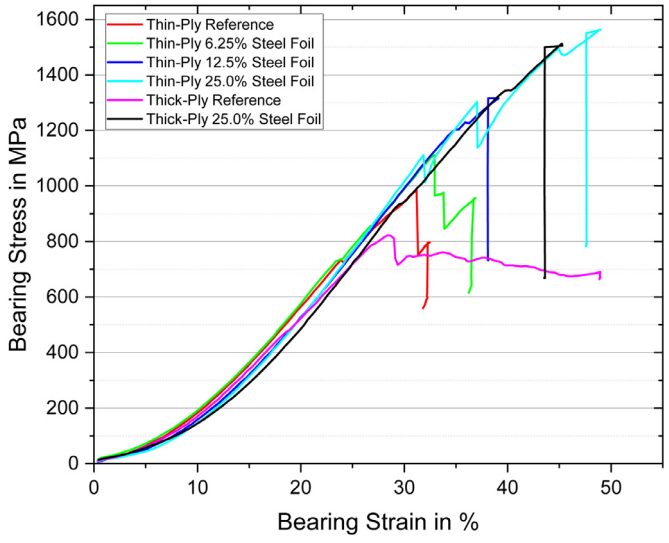

Fig. 10. Stress–strain-diagram of Thin-Ply, Thick-Ply and their hybrid configurations.

Ply specimens (magenta) show a progressive damage behavior and the Thin-Ply specimens (red) a brittle failure, stress reductions can be seen within the curves of the hybrid specimens within the test. For example, the curve of the Thin-Ply sample with a steel content of 25% (light blue) shows three stress reductions. The first occurs at 31.8%, the second at 37% and the third just before ultimate failure at 44.9%.

This development indicates that the material has been damaged. In order to investigate the damage process more in detail, samples were tested and stopped when the first decrease in stress was reached so that micrographs could be prepared and the damage mechanism responsible for the first drop in tensile stress could be observed. These micrographs are shown in Fig. 11. Fig. 11a shows a Thick-Ply sample with 25% stainless steel. Global buckling has formed, whereby the stainless steel layers have already deformed plastically. Fig. 11b shows a detailed view of the sample. The radii of the buckling are small which results in fibre fracture. Besides, the FML Thick-Ply samples show delamination at the interfaces between stainless steel and matrix. On one hand, delaminations can be caused by high shear stresses at the interface due to the high strain of the stainless steel. On the other hand, the stress in combination with initial damage can lead to out-of-plane stresses and thus enhance delamination growth. Besides the delaminations and the fibre breaks in the 0° layers, inter-fibre fractures occur in the ±45° layers. Larger radii show an intact fibre-matrix structure. Fig. 11d and e show a Thin-Ply sample with a 25% stainless steel content. Again, the first load drop indicates the first buckling. This buckling spreads out symmetrically from the centre of the sample to the outside and forms a kind of V-shaped wedge, as already observed with the FML Thick-Ply samples. As in Fig. 11 b, fibre breaks can be observed in the 0° layers in Fig. 11 e. Also, some ±45° layers of inter-fibre breaks show regions with plastic deformations. However, no delamination between stainless steel and matrix is visible. Due to the lower layer thicknesses and the associated higher number of interfaces, the shear stresses between the layers decrease, and delamination growth is suppressed. Fig. 11 c and f show a Thick-Ply sample without stainless steel and a Thin-Ply sample with 12.5% of stainless steel. Both samples show the typical failure behavior described above, global buckling exhibits from the mid-plane. With the Thick-Ply sample, it appears as if the 0° layers in the middle of the sample would fail under compression, initiating in the formation of buckling to the outside. This assumption confirms with the symmetrical damage.

Concerning the question of whether it makes sense to use fibre metal laminates for structural applications, it is not sufficient only to consider the maximum bearing strength. In the case of conventional construction materials such as metals, an offset bearing strength of 2% strain is the evaluation criterion. Therefore, three parameters are of particular importance in the case of bearing tests. The maximum bearing strength, the offset bearing strength and the stress at the first load drop, which is the first significant damage. All three parameters are shown in Fig. 12. The blue bars represent the strength at the time of the first measurable damage, the grey bars represent the offset bearing strength, and the black bars represent the maximum bearing strength. The Thick-Ply samples without stainless steel serve as reference material since they have the thicknesses commonly used today. However, the 160 gsm plies were laminated by block-scaling (four 40 gsm layers), so that the spreading process of the fibres also results in good quality in terms of fibre volume content, resin-rich regions and fibre angle deviation, which has a positive effect on compressive behavior [6,8]. The Thick-Ply samples show small differences between the first damage, the offset and the maximum bearing strength, but Thick-Ply samples exhibit a progressive damage behavior, so that even after the ultimate bearing strength, there is no risk of sudden failure. In comparison, the Thin-Ply samples without stainless steel have a higher offset and maximum bearing strength, but the stress of the first damage is at the same level as the Thick-Ply samples. Therefore, if the design guide tolerates no damage, the

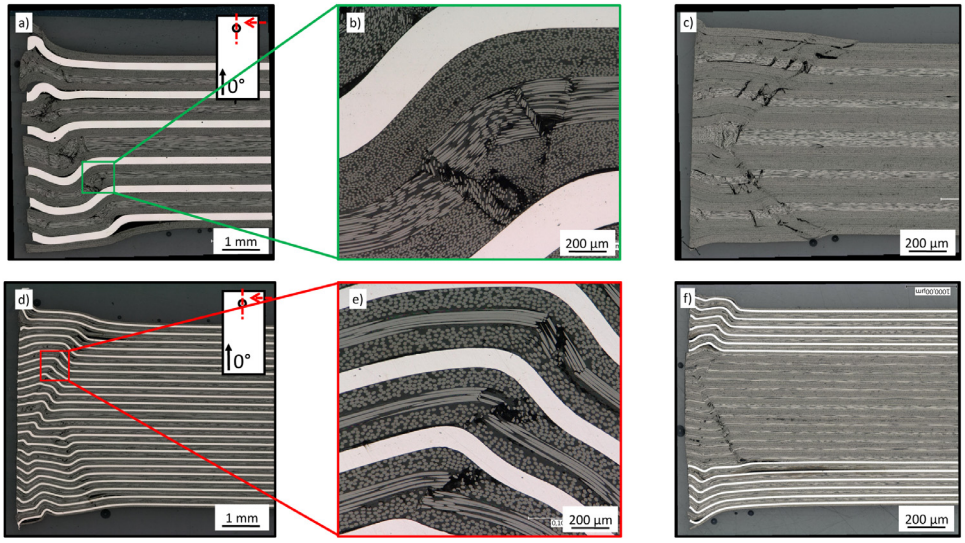

Fig. 11. Micrographs of samples tested until the first damage; a) Thick-Ply with 25% local steel content, b) Detailed view of micrograph a), c) Thin-Ply reference, d) Thin-Ply with 25% local steel content, e) Detailed views of micrograph d), f) Thin-Ply with 12.5% local steel content.

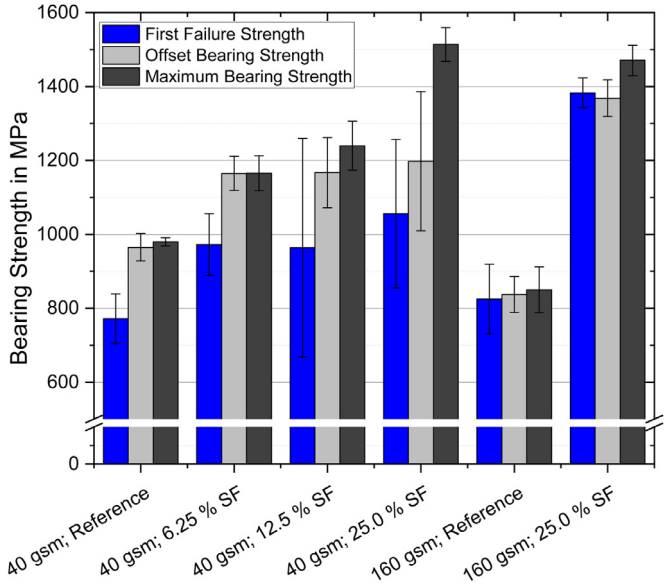

Fig. 12. First failure (blue), offset (grey) and maximum bearing (black) strength for neat and fibre metal laminates.

maximum allowable stress is equal to the Thick-Ply. However, after the first damage a high residual safety factor exists, as the maximum bearing strength is 26.96% higher. The hybrid laminates show significantly higher strengths regardless of the selected parameter. It is noticeable that the stress at the points of the first damage in all three FML Thin-Ply configurations have a similar value due to the high scattering. Also, the offset stress, which is above the stress of the first damage, is the same for all three configurations. A difference is visible in the maximum bearing strength, which increases significantly with increasing steel content. Compared to the Thin-Ply samples without steel, the maximum bearing strength of the Thin-Ply samples with 6.25% steel increases by 19.0%, with 12.5% by 26.5% and the thin FML samples with 25% by 54.6%. The difference between the sample configurations results in the residual safety factor after damage. With increasing steel content, the safety factor increases significantly. Whether first damages are tolerable would have to be checked in a further study under cyclic load. The Thick-Ply samples reinforced with stainless steel show the best results in terms of bearing strength. The maximum bearing strength is in the same range as the 25% Thin-Ply samples, but the parameters of the offset and the first damage increase significantly. The different damage mechanisms can be interpreted based on micrographs in Fig. 13.

Final failure of all configurations is due to buckling behind the specimen's support Buckling in the area of the clamping has a local load drop as a consequence but is not critical regarding the final failure. These local damages can be assigned to the stress reductions in the stress-strain diagrams. However, due to the side-wise support by the washers, the specimens do not fail at the first buckling and receive higher compressive stresses. The Thin-Ply FML specimens all have several global kink bands. It is noticeable that in the regions where the stainless steel foils replaced the 90° layers, the carbon layers are supported and show minor damage. Even at high deformations of the stainless steel, the supporting effect is maintained.

Especially the middle layers of the 6.25% (Fig. 13 a–c) and the 12.5% (Fig. 13 d–f) samples show significant damages in the area of neat CFRP. Broken fibres in the 0° layers indicate that the fibres have failed due to high compressive stresses. Due to the supporting effect of the stainless steel as well as the higher residual bending stiffness in the case of the thin layer thicknesses (see above), a local buckling does not result in a global failure. The results for the Thick-Ply FML samples show that the final failure results also in a buckling after the clamped area. In contrast, the buckling cannot be seen symmetrically from the middle, but the whole specimen buckles to one side. No buckling is found in the region of the clamping by the washes, as is the case with thinner layers. It can be seen that the first measurable damage, as shown in the bar chart, applies by higher stresses. This damage is probably the beginning of the final buckling behind the clamping area. However, smaller kink bands can be found in the 0° layers, which are caused by the high compressive loads. Due to the high bending stiffness of the thicker stainless steel foils, the 0° layers are still supported so that no global buckling occurs. In the front area of the sample, as shown in figure k), fibres broke and displaced locally that they form a kind of circle. These fibres are broken into small pieces and shifted into each other. Especially interesting are the ±45° layers, which in some layers show no visible damage and they are strongly deformed. This behavior would indicate that the matrix has deformed plastically, which is unusual for a fully cured epoxy resin.

In addition to the bearing strength, the weight and the geometry of the joint is an important factor. An improved strength taking into account four times the weight, as is the case with pure stainless steel, for example, would be practically meaningless. For this reason, the strengths should be viewed in relation to their weight, or in this case in relation to their density. Fig. 14 shows the global specific bearing strength. The global specific bearing strength is the quotient of the bearing strength and the global density of the tested sample. It can be seen

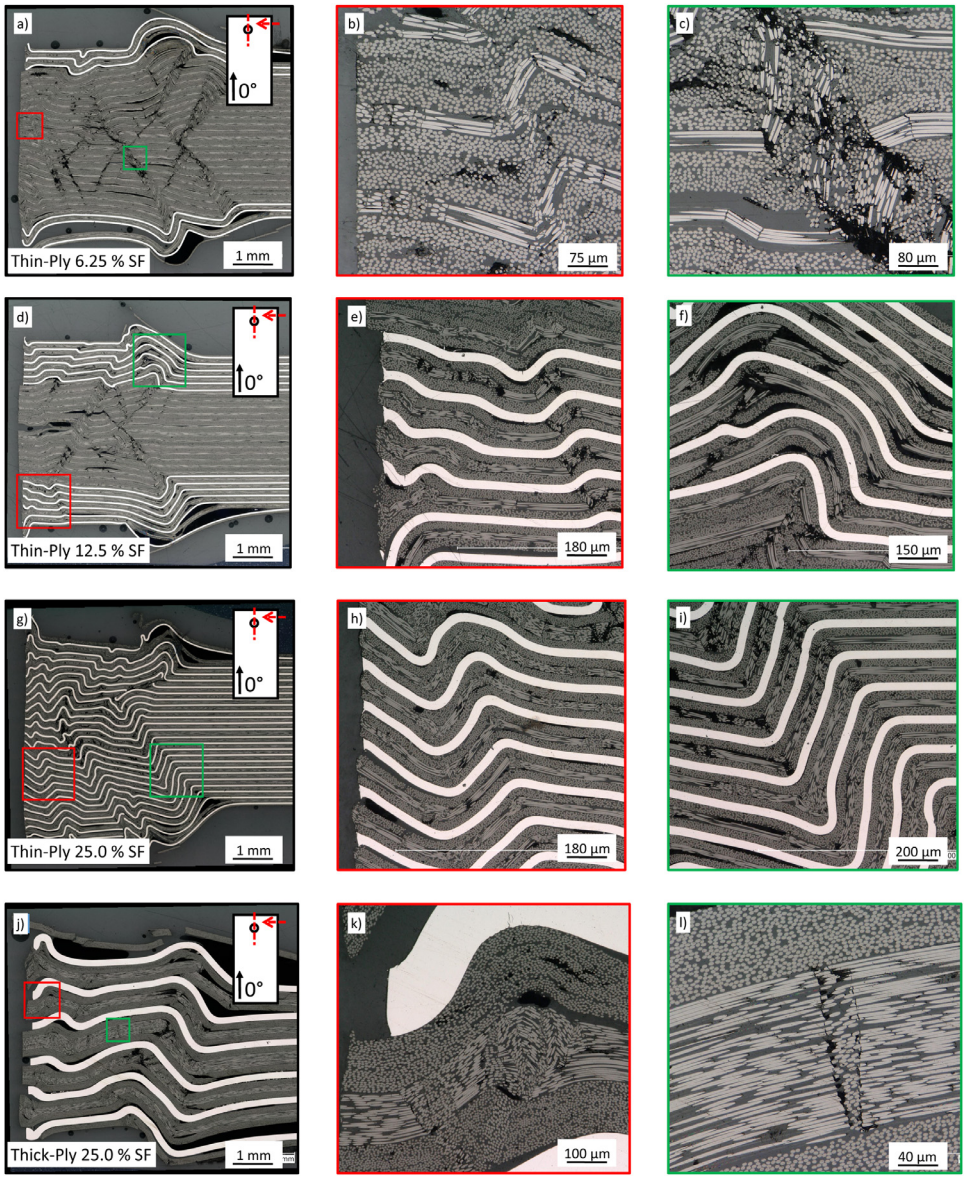

Fig. 13. Micrographs of hybrid fibre metal composite specimens after bearing tests; a–c) Thin-Ply with 6.25% local steel content, d–f) Thin-Ply 12.5% local steel content, g–i) Thin-Ply with 25% local steel content, j–l) Thick-Ply with 25% local steel content.

that the parameters of the three FML configurations approximate to the maximum specific bearing strength, but are still higher than those of the conventional specimens. With regard to the first failure, the results of the Thick-Ply samples with 25% stainless steel exhibit the highest values, whereby these correspond to the value of the offset and should be taken as the maximum for design. Due to the formation of delaminations, the propagation of damage is not as critical in static bearing tests, but probably have a strong effect on the fatigue bearing properties. This has to be clarified in further investigations, related to the Thin-Ply FML samples, the samples with a steel content of 6.25% show the highest specific strengths in first failure. The values are 35.5% above the specific first failure strength of the Thin-Ply samples and 26.0% above the Thick-Ply samples. In relation to the industrial application of the hybrid composites investigated here, it is shown that hybridisation with 6.25% stainless steel achieves the same specific maximum bearing strength and the highest specific offset bearing strength as the configurations with a higher steel content. Therefore, although the bearing strength increases with a higher steel content, this does not offer any further advantage concerning the lightweight design due to the increased weight, and thus in practice.

4. Conclusion

This study shows that the hybridisation of Thin-Ply CFRP laminates with stainless steel patches in areas of stress concentrations significantly increases open hole tensile and bearing strength. The previous limitation of the gap between unnotched strength and open hole tensile strength or rather bearing strength can be reduced, allowing the potential of thin plies to be applied in structural lightweight applications. In the case of the Thin-Ply samples with a local steel content of 25%, the open hole tension strength was increased by 64% and the bearing strength by 54.6% compared to the Thin-Ply sample without stainless steel. If the strengths are normalised to the global density of the sample, the increases are 36% for the specific open hole tension strength and 14% for the specific bearing strength. Micrographs of samples from both load cases show that the steel deformed plastically under high strains and was able to dissipate energy. Due to the plastic deformation and the supporting effect of the stainless steel against buckling, the specific strength is increased. Another limiting factor in the case of Thick-Ply FML laminates is the transition zone between stainless steel and CFRP. Due to the different stiffnesses and coefficients of thermal expansion,

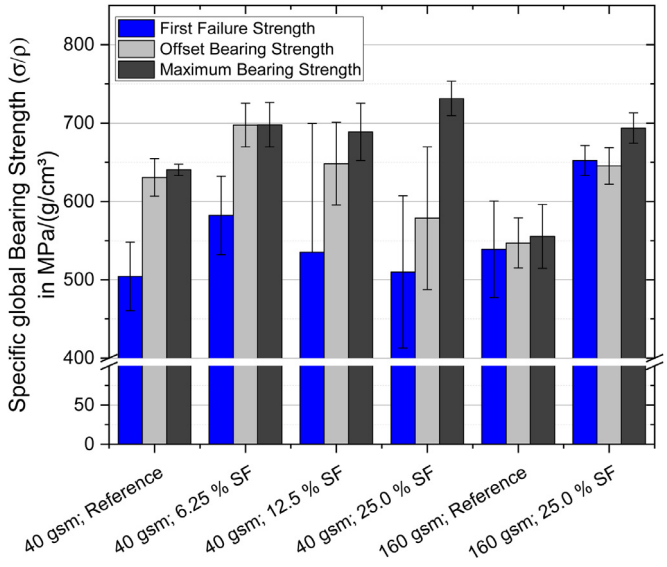

Fig. 14. Specific first failure, offset and maximum bearing strength.

stress concentrations occur, which initiate delamination in thicker layers and lead to premature failure. The use of thin-layer stainless steel foils and a step-wise arrangement of these foils leads to a smooth increase in stiffness over a larger area so that the stress concentrations are below the critical value for the formation of delamination. Thus higher open hole tensile strength is achieved. In the case of bearing performance, it was shown that concerning the density of the sample, an ideal local steel volume content of 6.25% was figured out. However, the bearing strength increases with higher steel content, but the density specific bearing strength does not increase because of the higher weight. Overall, the performance of CFRP Thin-Ply samples could be improved by using stainless steel foils as patches at stress concentrations and in the area of load introduction, demonstrating high potential for high performance structures.

Declaration of Competing Interest

The authors declare that they have no known competing financial interests or personal relationships that could have appeared to influence the work reported in this paper.

References

[1] M.C.-Y. Niu, Composite Airframe Structures: Practical Design Information and Data, 3rd, Conmilit Press, Hong Kong, 2000.
[2] K. Kawabe, S. Tomoda, T. Matsuo, A pneumatic process for spreading reinforcing fiber tow, in: Proceedings of the 42nd International SAMPE Symposium, 1997, pp. 65–76.
[3] S. Sihn, R. Kim, K. Kawabe, S. Tsai, Experimental studies of thin-ply laminated composites, Compos. Sci. Technol. 67 (6) (2007) 996–1008, doi:10.1016/j.compscitech.2006.06.008.
[4] A. Arteiro, C. Furtado, G. Catalanotti, P. Linde, P.P. Camanho, Thin-ply polymer composite materials: a review, Compos. Part A: Appl. Sci. Manuf. 132 (2020) 105777, doi:10.1016/j.compositesa.2020.105777.
[5] M.R. Wisnom, B. Khan, S.R. Hallett, Size effects in unnotched tensile strength of unidirectional and quasi-isotropic carbon/epoxy composites, Compos. Struct. 84 (1) (2008) 21–28, doi:10.1016/j.compstruct.2007.06.002.
[6] R. Amacher, J. Cugnoni, J. Botsis, L. Sorensen, W. Smith, C. Dransfeld, Thin ply composites: experimental characterization and modeling of size-effects, Compos. Sci. Technol. 101 (101) (2014) 121–132, doi:10.1016/j.compscitech.2014.06.027.
[7] J. Cugnoni, R. Amacher, S. Kohler, J. Brunner, E. Kramer, C. Dransfeld, W. Smith, K. Scobbie, L. Sorensen, J. Botsis, Towards aerospace grade thin-ply composites: effect of ply thickness, fibre, matrix and interlayer toughening on strength and damage tolerance, Compos. Sci. Technol. 168 (2018) 467–477, doi:10.1016/j.compscitech.2018.08.037.
[8] T. Yokozeki, Y. Aoki, T. Ogasawara, Experimental characterization of strength and damage resistance properties of thin-ply carbon fiber/toughened epoxy laminates, Compos. Struct. 82 (3) (2008) 382–389, doi:10.1016/j.compstruct.2007.01.015.
[9] J. Studer, A. Keller, F. Leone, D. Stefaniak, C. Dransfeld, K. Masania, Local reinforcement of aerospace structures using co-curing RTM of metal foil hybrid composites, Prod. Eng. 12 (2) (2018) 195–201, doi:10.1007/s11740-018-0794-3.
[10] K. Masania, R. Geissberger, D. Stefaniak, C. Dransfeld, Steel Foil Reinforced Composites: Experimental and Numerical Study of Strength, Plasticity and Ply Size Effect, 2015.
[11] B. Kötter, J. Karsten, J. Körbelin, B. Fiedler, Cfrp thin-ply fibre metal laminates: influences of ply thickness and metal layers on open hole tension and compression properties, Materials 13 (4) (2020), doi:10.3390/ma13040910.
[12] B. Bosbach, M. Baytekin-Gerngross, E. Sprecher, J. Wegner, M.-D. Gerngross, J. Carstensen, R. Adelung, B. Fiedler, Maximizing bearing fatigue lifetime and CAI capability of fibre metal laminates by nanoscale sculptured al plies, Compos. Part A: Appl. Sci. Manuf. 117 (2019) 144–155, doi:10.1016/j.compositesa.2018.11.017.
[13] G. Kolks, K.I. Tserpes, Efficient progressive damage modeling of hybrid composite/titanium bolted joints, Compos. Part A: Appl. Sci. Manuf. 56 (2014) 51–63, doi:10.1016/j.compositesa.2013.09.011.
[14] J. Both, M. Wedekind, H. Baier, Simulation and experimental characterization of the bearing behaviour of CFRP-metall laminates, in: Proceedings of the 15th European Conference on Composites, 2012, pp. 1–7. Venice
[15] P.P. Camanho, F.L. Matthews, Stress analysis and strength prediction of mechanically fastened joints in FRP: a review, Compos. Struct. 28 (1997) 529–547.
[16] P.P. Camanho, C. Tavares, R. de Oliveira, A.T. Marques, A. Ferreira, Increasing the efficiency of composite single-shear lap joints using bonded inserts, Compos. Part B: Eng. 36 (5) (2005) 372–383, doi:10.1016/j.compositesb.2005.01.007.
[17] G. Catalanotti, P.P. Camanho, A semi-analytical method to predict net-tension failure of mechanically fastened joints in composite laminates, Compos. Sci. Technol. 76 (2013) 69–76, doi:10.1016/j.compscitech.2012.12.009.
[18] A. Fink, P.P. Camanho, J.M. Andrés, E. Pfeiffer, A. Obst, Hybrid CFRP/titanium bolted joints: performance assessment and application to a spacecraft payload adaptor, Compos. Sci. Technol. 70 (2) (2010) 305–317, doi:10.1016/j.compscitech.2009.11.002.
[19] A. Crosky, D. Kelly, R. Li, X. Legrand, N. Huong, R. Ujjin, Improvement of bearing strength of laminated composites, Compos. Struct. 76 (3) (2006) 260–271, doi:10.1016/j.compstruct.2006.06.036.
[20] R. Li, N. Huong, A. Crosky, A.P. Mouritz, D. Kelly, P. Chang, Improving bearing performance of composite bolted joints using z-pins, Compos. Sci. Technol. 69 (7-8) (2009) 883–889, doi:10.1016/j.compscitech.2008.12.005.
[21] E. Petersen, D. Stefaniak, C. Hühne, Experimental investigation of load carrying mechanisms and failure phenomena in the transition zone of locally metal reinforced joining areas, Compos. Struct. 182 (2017) 79–90, doi:10.1016/j.compstruct.2017.09.002.
[22] 3M Aerospace and Aircraft Maintanance Division, 3M Surface Pre-Treatment AC-130, 2012.
[23] W.-H. Chen, S.-S. Lee, J.-T. Yeh, Three-dimensional contact stress analysis of a composite laminate with bolted joint, Compos. Struct. 30 (1995) 287–297.
[24] P.P. Camanho, M. Lambert, A design methodology for mechanically fastened joints in laminated composite materials, Compos. Sci. Technol. 66 (15) (2006) 3004–3020, doi:10.1016/j.compscitech.2006.02.017.
[25] C. Cooper, G.J. Turvey, Effects of joint geometry and bolt torque on the structural performance of single bolt tension joints in pultruded GRP sheet material, Compos. Struct. 32 (1995) 217–226.
[26] D30 Committee, Test Method for Open-Hole Tensile Strength of Polymer Matrix Composite Laminates, ASTM D 5766-02, 2002, 10.1520/D5766_D5766M-11R18
[27] D30 Committee, Test Method for Bearing Response of Polymer Matrix Composite Laminates, ASTM D 5961-01, 2001, 10.1520/D5961_D5961M-17
[28] D30 Committee, Test Method for Tensile Properties of Polymer Matrix Composite Materials, ASTM D 3039-00, 2000, 10.1520/D3039_D3039M-17
[29] E28 Committee, Test Methods of Tension Testing of Metallic Foil, ASTM e345-16, 2016, 10.1520/E0345-16
[30] S.P. Garbo, J.M. Ogonowski, Effect of variances and manufacturingtolerances on the design strength and life of mechanically fastenedcomposite joints, Tech. Rep. AFWAL-TR-81-3041, vol. 1, McDonnell Aircraft Company, 1981. Final Report AFWAL-TR-81-3041.
[31] A. Arteiro, G. Catalanotti, J. Xavier, P.P. Camanho, Notched response of non-crimp fabric thin-ply laminates: Analysis methods, Compos. Sci. Technol. 88 (2013) 165–171, doi:10.1016/j.compscitech.2013.09.003.
[32] P.P. Camanho, Application of Numerical Methods to the Strength Prediction of Mechanically Fastened Joints in Composite Laminates, Imperial College of Science, London, 1999 Dissertation.